

Exploring jet interactions in the quark-gluon plasma using jet substructure measurements in Pb-Pb collisions with ALICE

Raymond Ehlers* on behalf of the ALICE Collaboration

Lawrence Berkeley National Laboratory/UC Berkeley

E-mail: raymond.ehlers@cern.ch

Jets are generated in hard interactions in high-energy nuclear collisions. Jets propagate through the quark-gluon plasma (QGP) as the jet shower evolves; their interaction with the QGP, known as jet quenching, generates observable phenomena that provide incisive probes of the structure and dynamics of the QGP. For instance, medium-induced modification of jet substructure probes color coherence, and may be sensitive to differences in quark and gluon energy loss due to their different Casimir factors. Jet grooming can be used to focus on specific regions of phase space, isolating medium-induced effects on hard splittings in the jet shower. ALICE is well suited for such substructure measurements due to its precise charged-particle tracking, which enables high-efficiency measurements of narrow splittings in jets down to low transverse momentum. In these proceedings several recent jet substructure measurements in Pb-Pb collisions at $\sqrt{s_{NN}} = 5.02$ TeV are reported, for both ungroomed jets and jets that have been groomed using the Soft Drop and Dynamical Grooming algorithms. Measurements of the groomed jet radius, $\theta_g \equiv R_g/R$; the groomed jet momentum fraction, z_g ; and the groomed relative transverse momentum, $k_{T,g}$ are reported. These measurements show direct evidence of modification of the angular structure of jets in the QGP, and provide new constraints on the search for large-angle scattering of jets off of quasi-particles by interaction with the QGP. New measurements of sub-jet fragmentation, generalized jet angularities, and jet-axis differences, which provide insight into the angular and momentum structure of modified jets are also presented. Comparisons to model calculations are discussed.

*41st International Conference on High Energy physics - ICHEP2022
6-13 July, 2022
Bologna, Italy*

*Speaker

1. Introduction

High momentum-transfer processes in high energy nuclear collisions generate collimated sprays of particles known as jets. As jets propagate through the quark-gluon plasma (QGP) formed in these collisions, their interactions encode properties of the medium via modification of jet properties and structure, in a process known as jet quenching. The measurement of jet substructure observables, and their comparison to theoretical calculations, can isolate and quantify these modifications, providing insight into QGP properties.

The ALICE experiment [1] is well-suited for such substructure measurements. ALICE is able to measure small jet splitting angles with high precision, due to precise charged-particle tracking down to low particle transverse momentum (p_T) using the Inner Tracking System and Time Projection Chamber. ALICE also measures jets to the lowest $p_{T,\text{jet}}$ at the LHC, where modifications due to the medium are largest relative to the momentum scale of the probe. These capabilities enable a broad jet substructure program.

Jets are reconstructed using the anti- k_T algorithm implemented in FastJet [2]. All results presented here are based on charged-particle jets, which utilize charged particles for jet reconstruction. Jet finding in pp and Pb–Pb collisions at $\sqrt{s_{NN}} = 5.02$ TeV is performed using jet resolution parameters $R = 0.2$ and 0.4 . The data were recorded during the 2017 and 2018 LHC runs. Jet candidates selected for further analysis are required to be contained fully within the fiducial acceptance, with background contributions in Pb–Pb collisions subtracted via constituent subtraction [3].

After jet selection, jet substructure is measured using both groomed and ungroomed approaches. Groomed substructure removes soft, wide-angle emissions to isolate the hardest splittings, while ungroomed substructure probes the entire splitting phase space, including soft emissions. In the groomed approach, each jet is first reclustered using the Cambridge-Aachen (C/A) algorithm. This declustered splitting tree is then used as input for a grooming algorithm, which searches through the tree and selects splittings according to specific criteria. For the results presented in these proceedings, groomed observables utilize either 1) the Soft Drop (SD) grooming algorithm with a minimum shared momentum fraction requirement, z_{cut} [4], or 2) the Dynamical Grooming (DyG) algorithm with dynamic hardness measure a , which can be used to focus on, e.g., the largest k_T ($a = 1.0$) [5]. The observable is then calculated using the properties of the selected splitting. In the ungroomed approach, the jet constituents or declustered splitting tree are directly analysed to calculate the observable of interest. In both cases, observables are corrected for detector effects and background fluctuations with two-dimensional unfolding in $p_{T,\text{jet}}$ and the substructure observable using Bayesian iterative unfolding implemented in RooUnfold [6].

2. Summary substructure observables

Substructure observables which characterize the substructure of the entire jet via a single value are referred to as “summary substructure” observables. One such example is the angle between jet axes determined using different jet recombination and grooming algorithms [7]. By using the entire jet, this observable is sensitive to the distribution of soft radiation at large angles. To construct this observable, charged-particle jets are reconstructed as usual using E recombination scheme, which defines the standard jet axis. Each jet is then reclustered using the C/A algorithm, utilizing either

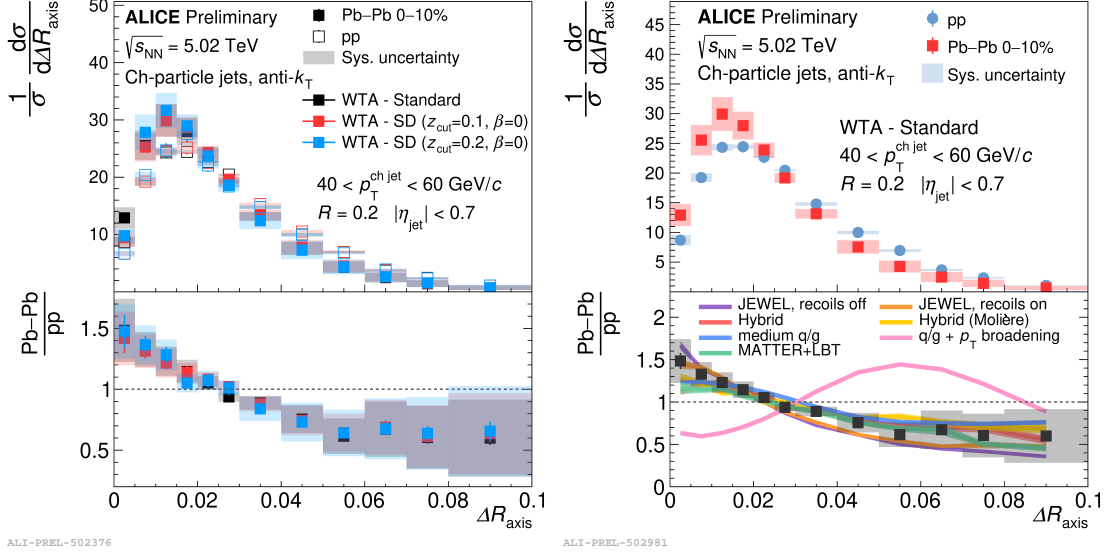


Figure 1: Jet axis difference for various axis definitions (left), compared to models for WTA vs standard jet axes (right), for charged-particle jets with $R = 0.2$ in $40 < p_{T,jet}^{ch} < 60$ GeV/c in pp and 0–10% central Pb–Pb collisions at $\sqrt{s_{NN}} = 5.02$ TeV.

SD with $z_{cut} > 0.1$ or 0.2 to define the SD axis, or alternatively, the Winner-Take-All (WTA) p_T recombination scheme. The observable, $\Delta R_{axis} = \sqrt{(y_1 - y_2)^2 + (\varphi_1 - \varphi_2)^2}$, is then defined as the angular difference between the directions of two axes.

Results are shown in Fig. 1 for charged-particles jets with $R = 0.2$ in $40 < p_{T,jet}^{ch} < 60$ GeV/c. In all jet axis combinations (Fig. 1, left), the difference between WTA and the other axis definitions is narrower in central (0–10%) Pb–Pb than in pp collisions. The modification is qualitatively described by a wide variety of models (Fig. 1, right) despite those models utilizing different physics mechanisms to reproduce the data, such as color coherence or changing the quark and gluon fractions in the medium.

Jet substructure can also be characterized by generalized angularities, which summarize the substructure via a p_T -weighed sum of the angular distribution of the jet constituents. These angularities are defined as $\lambda_\alpha^\kappa = \sum_i z_i^\kappa \theta_i^\alpha$, where α and κ are continuous parameters [8]. The ALICE measurements are focused on $\kappa = 1$ and $\beta > 0$, which ensures infrared and collinear safety. For the groomed case, which reduces intra-jet broadening and recoil effects, the constituents of the subjet pair that passes the SD condition of $z_{cut} > 0.2$ are used to calculate the angularities. Figure 2 shows the ratio of angularities with $\alpha = 1, 1.5, 2,$ and 3 for $R = 0.2$ jets with $40 < p_{T,jet}^{ch} < 60$ GeV/c, in central (0–10%) Pb–Pb and pp collisions. Ungroomed angularities are shown on the left, while groomed angularities are shown on the right. Both exhibit a narrowing trend in Pb–Pb collisions, with smaller uncertainties and clearer narrowing in the groomed case. Many models quantitatively describe the data (not shown), with similar performance as for the jet axis difference.

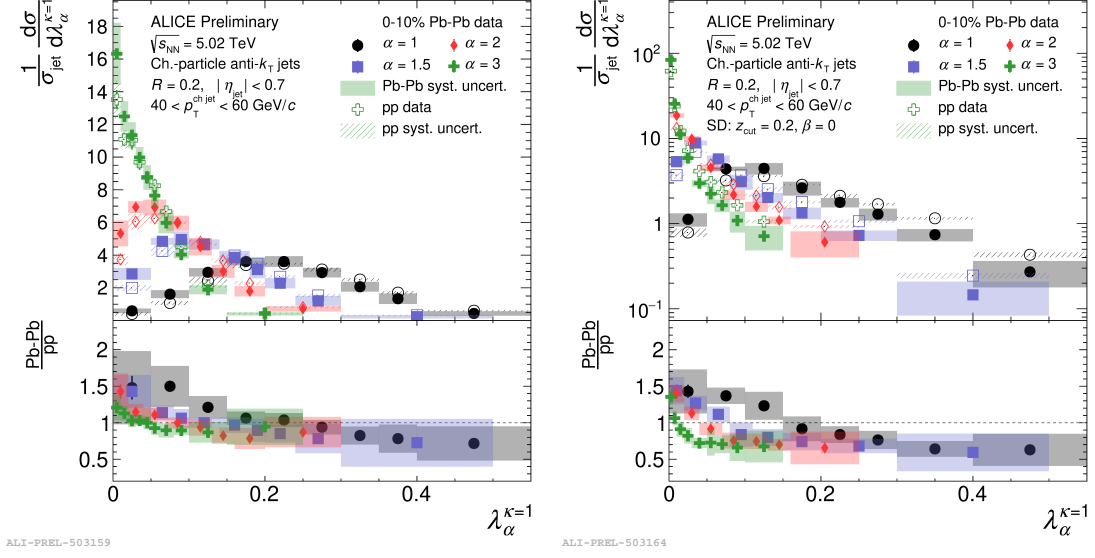


Figure 2: Generalized angularities for charged-particle jets with $R = 0.2$ in $40 < p_{T,\text{jet}}^{\text{ch}} < 60$ GeV/c, measured in pp and 0–10% central Pb–Pb collisions at $\sqrt{s_{\text{NN}}} = 5.02$ TeV. Ungroomed angularities are shown on the left, while groomed angularities are shown on the right.

3. Subject observables

Another approach to studying jet substructure is to characterize the properties of subjects found via declustering with the C/A algorithm. As one example, ALICE has characterized the groomed momentum splitting fraction z_g and jet radius R_g for jets groomed with SD $z_{\text{cut}} > 0.2$ [9]. This study found no modification of z_g , while R_g was found to have an enhancement of narrow splittings and a suppression of wide splittings, corresponding to a promotion of narrow subjects or a filtering of wide subjects. This narrowing is consistent with the jet axis difference and generalized angularities.

Substructure can also be used to search for point-like (Moliere) scattering centers in the medium [10, 11]. Such scattering centers have been predicted to enhance the distribution of high relative transverse momentum emissions, k_T , in Pb–Pb compared to pp collisions. To search for such an effect, we decluster each jet candidate and utilize grooming algorithms to identify hard splittings, including SD with $z_{\text{cut}} > 0.2$, as well DyG with $a = 0.5, 1.0, \text{ and } 2.0$. For each identified splitting, the observable is calculated as $k_{T,g} = p_{T,2} \sin \Delta R$, where $p_{T,2}$ is the p_T of the softer subject and ΔR is the angle between the subjects.

The measurement of $k_{T,g}$ using various grooming methods in 30–50% semi-central Pb–Pb collisions for $R = 0.2$ charged-particle jets measured in $60 < p_{T,\text{jet}}^{\text{ch}} < 80$ GeV/c is shown on the left of Fig. 3. This is the first measurement using DyG in heavy-ion collisions, enabled by removing the soft k_T contribution via the requirement of a minimum measured $k_T > 1$ GeV/c. All of the methods are consistent within uncertainties, suggesting that they are selecting the same set of splittings at high $k_{T,g}$. The right side of Fig. 3 shows a comparison of the spectra measured in pp and 30–50% semi-central Pb–Pb collisions for the same jet selections using SD with $z_{\text{cut}} > 0.2$. The z_{cut} in the SD grooming allows for the removal of the minimum k_T requirement, which enables measuring over a larger range in $k_{T,g}$. The apparent modification is consistent with the narrowing observed

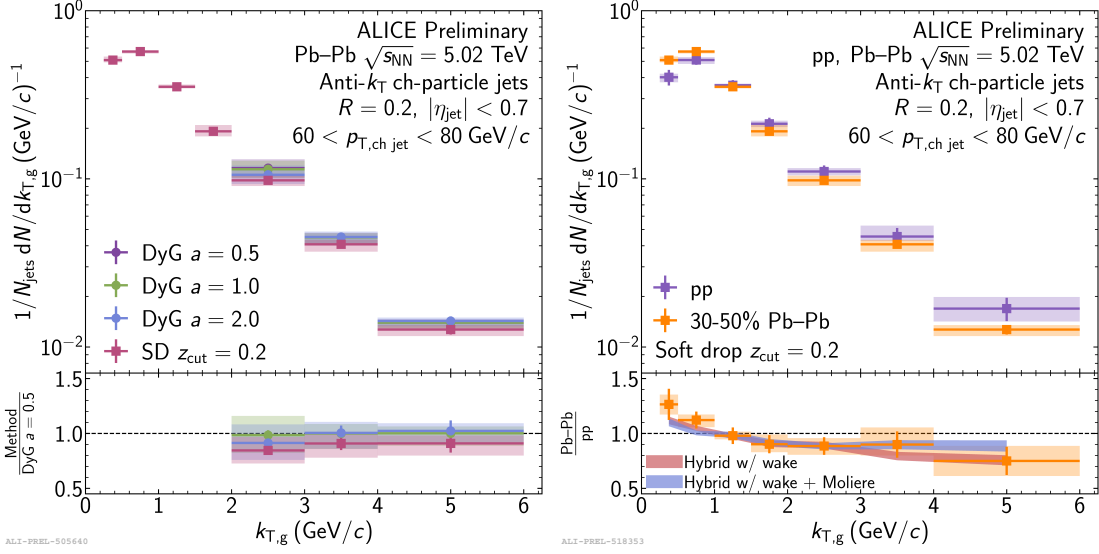


Figure 3: A comparison of hardest $k_{T,g}$ splittings for a variety of grooming methods measured in 30–50% semi-central Pb–Pb collisions at $\sqrt{s_{NN}} = 5.02$ TeV is shown on the left, while a comparison of $k_{T,g}$ measured in pp and Pb–Pb collisions for Soft Drop with $z_{cut} > 0.2$ is shown on the right. Both panels show $R = 0.2$ charged-particle jets measured in $60 < p_{T,jet}^{ch} < 80$ GeV/c.

in R_g , meaning that any possible point-like scattering effects are convolved with this narrowing. Based on the comparison with the Hybrid model [11], this measurement does not yet have sufficient precision to be sensitive to the effects of Moliere scattering.

Ungroomed subjects can probe harder fragmentation than is accessible solely via single hadrons. By reclustering $R = 0.4$ jets using the anti- k_T algorithm with subjet resolution parameter r , hard subjet properties can be investigated. This study focuses on the subjet fragmentation, $z_r = \frac{p_{T,subjet}^{ch}}{p_{T,jet}^{ch}}$, for the leading subjet identified in each jet [12]. Figure 4 shows the ratio of subjet fragmentation in 0–10% central Pb–Pb to that in pp collisions for $r = 0.1$ (0.2) on the left (right). The data are consistent with no modification in Pb–Pb collisions, although there is a hint of a change of shape as $z_r \rightarrow 1$ for $r = 0.1$. The interplay between the softening at mid z_r due to medium-induced radiation and the hardening at high z_r due to differences in the quark and gluon fractions may lead to a similar non-trivial shape change. Both the medium jet functions [13, 14] and JETSCAPE [15–17] curves describe the data fairly well within their range of applicability, while JEWEL [18, 19] is not consistent with the data except for $r = 0.1$ with recoils on.

4. Summary

ALICE has measured a wide variety of ungroomed and groomed jet substructure observables in Pb–Pb and pp collisions at $\sqrt{s_{NN}} = 5.02$ TeV. Although there is no modification of the groomed momentum splitting fraction z_g , a narrowing effect is seen for substructure observables with an angular dependence. The underlying mechanism is still under investigation, with possibilities including color coherence, changes in the quark and gluon fractions in the medium, and bias towards narrower jets surviving transversal of the medium. The distribution of groomed relative

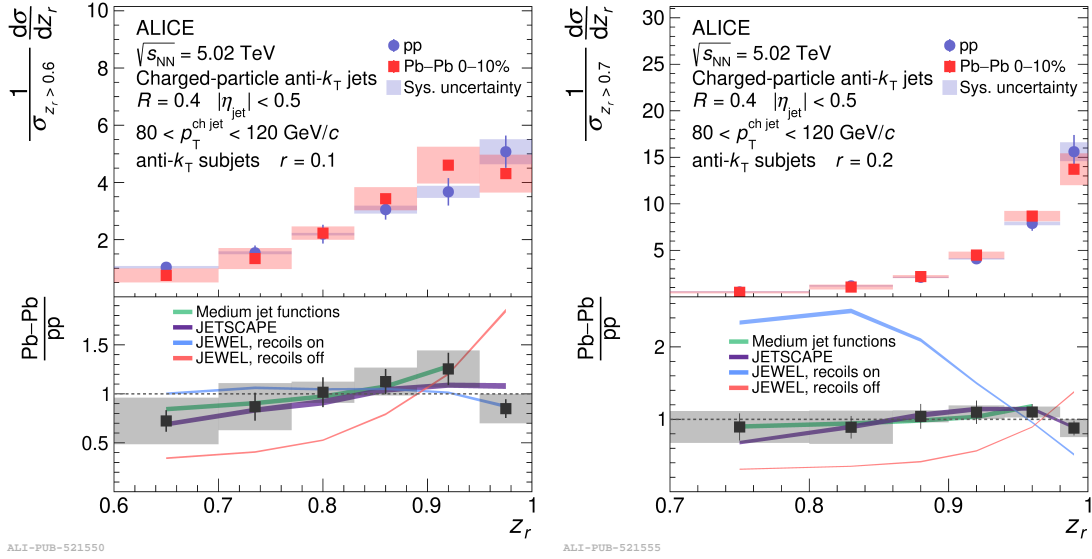


Figure 4: The ratio of subjet z measured in pp and 0–10% central Pb–Pb collisions at $\sqrt{s_{\text{NN}}} = 5.02$ TeV for $R = 0.4$ charged-particle jets measured in $80 < p_{\text{T,jet}}^{\text{ch}} < 120$ GeV/ c . The measurement for $r = 0.1$ is shown on the left, while $r = 0.2$ is shown on the right.

transverse momentum, $k_{\text{T,g}}$, is the first application of Dynamical Grooming in heavy-ion collisions. However, it is not yet precise enough to be able to observe effects from Moliere scattering.

References

- [1] ALICE collaboration *Int. J. Mod. Phys. A* **29** (2014) 1430044 [arxiv:1402.4476].
- [2] M. Cacciari, G.P. Salam and G. Soyez *Eur. Phys. J. C* **72** (2012) 1896 [arxiv:1111.6097].
- [3] P. Berta, L. Masetti, D.W. Miller and M. Spousta *JHEP* **2019** (2019) 175 [arxiv:1905.03470].
- [4] A.J. Larkoski, S. Marzani, G. Soyez and J. Thaler *JHEP* **05** (2014) 146 [arxiv:1402.2657].
- [5] Y. Mehtar-Tani, A. Soto-Ontoso and K. Tywoniuk *Phys. Rev. D* **101** (2020) 034004 [arxiv:1911.00375].
- [6] T. Auyeub *arXiv* 1105.1160 [arxiv:1105.1160].
- [7] P. Cal, D. Neill, F. Ringer and W.J. Waalewijn *JHEP* **04** (2020) 211 [arxiv:1911.06840].
- [8] A.J. Larkoski, J. Thaler and W.J. Waalewijn *JHEP* **11** (2014) 129 [arxiv:1408.3122].
- [9] ALICE collaboration *Phys. Rev. Lett.* **128** (2022) 102001 [arxiv:2107.12984].
- [10] F. D’Eramo, M. Lekaveckas, H. Liu and K. Rajagopal *JHEP* **2013** (2013) 31 [arxiv:1211.1922].
- [11] F. D’Eramo, K. Rajagopal and Y. Yin *JHEP* **01** (2019) 172 [arxiv:1808.03250].
- [12] ALICE collaboration *arXiv* 2204.10270 [arxiv:2204.10270].
- [13] Z.-B. Kang, F. Ringer and W.J. Waalewijn *JHEP* **07** (2017) 064 [arxiv:1705.05375].
- [14] J.-W. Qiu, F. Ringer, N. Sato and P. Zurita *Phys. Rev. Lett.* **122** (2019) 252301 [arxiv:1903.01993].
- [15] JETSCAPE collaboration *arXiv* 1903.07706 [arxiv:1903.07706].
- [16] A. Majumder *Phys. Rev. C* **88** (2013) 014909 [arxiv:1301.5323].
- [17] Y. He, T. Luo, X.-N. Wang and Y. Zhu *Phys. Rev. C* **91** (2015) 054908 [arxiv:1503.03313].
- [18] K.C. Zapp, F. Krauss and U.A. Wiedemann *JHEP* **03** (2013) 080 [arxiv:1212.1599].
- [19] K.C. Zapp *Eur. Phys. J. C* **74** (2014) 2762 [arxiv:1311.0048].